Supplement of Atmos. Chem. Phys., 19, 3025–3042, 2019
https://doi.org/10.5194/acp-19-3025-2019-supplement


Atmospheric Chemistry and Physics
Open Access
EGU

*Supplement of*

# Causes of a continuous summertime $O_3$ pollution event in Jinan, a central city in the North China Plain

**Xiaopu Lyu et al.**

*Correspondence to:* Hai Guo (ceguohai@polyu.edu.hk)

**Text S1** Validation of the WRF-CMAQ modeling

Due to the inevitable uncertainties inherent in chemical transport models, such as the uncertainties in emission inventory, meteorological simulation and chemical mechanisms (Hu et al., 2016), it is difficult to deduce the reasons of the discrepancies between the simulated and observed $O_3$ mixing ratios. However, the observations indicated extremely high levels of some VOCs on the three days when $O_3$ values were under-predicted. Specifically, 13.5 ppbv of ethene was observed at 14:00 LT on August 1. On August 7, 5.6 ppbv of isoprene, 16.2 ppbv of HCHO and 2.3 ppbv of hexanal were measured during 12:00 – 14:00 LT. On August 10, 22.7 ppbv of propene and 12.7 ppbv of *i*-butane were recorded at 08:00 and 16:00 LT, respectively. It is noteworthy that these mixing ratios were 5 – 10 times higher than the average mixing ratios of these VOCs. Further, most of these VOCs are highly reactive in $O_3$ photochemistry and may make great contributions to local $O_3$ production. With the setting of constant emissions of $O_3$ precursors, WRF-CMAQ did not reproduce these extremely high levels of VOCs, which was a plausible reason for the under-prediction of $O_3$ on August 1, 7 and 10. Ji'nan was behind a low pressure trough on August 9 – 10. However, vertical transport was simulated to make negative contributions to $O_3$ between 10:00 LT and 18:00 LT on August 10, according to the process

analysis. In addition, the simulated $O_3$ in the upper atmosphere on August 10 was relatively low compared to that on August 5, 6 and 9 (Figure S9). Namely, the model might fail to reproduce the $O_3$ enhancement driven by the low pressure trough on August 10.

The process analysis indicated that horizontal and vertical transport dominated the sources of $O_3$ at noon (10:00-12:00 LT) and the other time periods on July 20, respectively. While vertical transport explained the high $O_3$ at night (Figure 2), it was not likely that horizontal transport built up $O_3$ at noon, because the southwesterly airflows were originated from South China and passed central China (Figure 4), where $O_3$ values were relatively low on that day (high $O_3$ occurred in Hebei province to the northwest of Ji'nan). Therefore, the overestimate of the transport effect led to the higher simulated $O_3$ on July 20.

Despite these discrepancies, overall the observed $O_3$ at the sampling site was well reproduced. In addition, the spatial distribution of the simulated $O_3$ was highly consistent with the observed $O_3$ distribution, as shown in Figure S10. The average concentrations of the simulated VOCs were also compared with the observations (Figure S11). While the day-to-day and diurnal variations of the observed VOCs were not well reproduced (not shown), which is a proverbial drawback of the WRF-CMAQ, the model reasonably simulated the magnitudes of VOCs. Moreover, the averages of the observations (Avg. Obs.) and simulations (Avg. Sim.), difference between Avg. Obs. and Avg. Sim. (Diff.), root mean square error (RMSE), normalized mean bias (NMB), normalized mean error (NME) and index of agreement (IOA) were calculated to reflect the agreements between the simulated and observed temperature (Temp.), relative humidity (R.H.), wind speed (W.S.), pressure (Press.), $NO_2$ and $O_3$, as listed in Table S4. Generally, the lower Diff., RMSE, NMB and NME, but higher IOA indicate better agreement between the simulated and observed values (Willmott et al., 1985). The validation of the simulations of air pollutants was carried out at 8 AQMSs of CNEMC in and around Ji'nan, and at the sampling site, while the meteorological parameters monitored at 6 airports in eastern and northern China and at the sampling site were used to validate the simulated meteorological conditions. The metrics calculated in this study were well within the ranges of those reported in previous studies involving WRF-CMAQ simulations (Table S4) (Jiang et al., 2010; Wang et al., 2015), suggesting good performance of the model in reproducing the meteorological conditions and air pollutants. Thus, the simulated results were accepted for further analyses.

**Text S2** Source apportionment of $O_3$ precursors

The positive matrix factorization (PMF) model was employed to identify the sources of $O_3$ precursors. Details about the operation principles of PMF can be found in Paatero and Tapper (1994). Briefly, the model treats the matrix of input concentrations as the product of two matrixes (*i.e.*, factor contribution and factor profile). Here, hourly concentrations of 31 VOCs, CO, NO and $NO_2$ in 54 samples were input into the model. The VOCs applied for source apportionment (termed as VOCs* hereafter) were either tracers of specific sources (*e.g.*, isoprene for biogenic emissions), or having high concentrations (detectable in at least 80% samples). On average, VOCs* accounted for 79.5±11.7% of the total quantified VOCs. The uncertainties of the input concentrations of $O_3$ precursors were set as $\frac{5}{6} \times \mathrm{DL}$ and $\sqrt{(10\% \times concentration)^2 + (0.5 \times DL)^2}$ for the concentrations lower than and higher than DLs, respectively.

The model was run for 20 times with a random seed and the best resolution automatically given by the model was accepted. A total of 6 sources of $O_3$ precursors were resolved by PMF in this study. The number of sources was chosen based on the criteria that the tracers indicating different sources were not allocated in the same source, and all the sources were interpretable according to the tracers. The Bootstrap method integrated in PMF was used to estimate the uncertainties of the modelling results.

Figure S13 shows the profiles of the six sources of $O_3$ precursors extracted from PMF. The first source contained high levels of *n*/*i*-pentanes and aromatics, likely representing gasoline exhaust (Ho et al., 2009; Ling and Guo, 2014). The heavy hydrocarbons (C8-C10) dominated the second source, with great abundances of the combustion tracers, such as $C_2$-$C_3$ hydrocarbons, CO, NO and $NO_2$. These are in line with the features of diesel exhaust (Liu et al., 2008). The third source was assigned as BVOC, due to the exclusively high loading of isoprene (Guenther, 2006). The fourth source was rich in $C_4$ hydrocarbons, including *n*/*i*-butanes and 1,3-butadiene. It was defined as liquefied petroleum gas (LPG) usage, since butanes and butenes are present in large quantities in China's LPG (Song et al., 2008 and references therein). Solvent usage was represented by the fifth source, in view of the high loadings of hexane isomers (2,3-dimethylbutane, 2-methylpentane and 3-methylpentane) and moderate loadings of *n*-hexane, toluene, ethylbenzene and xylenes (Guo et al., 2011). At last, most of styrene, benzene, toluene, exthylbenzene and xylenes were allocated to the sixth source, which also contained moderate levels of light ($C_2$-$C_5$) hydrocarbons. Since styrene is a common

petrochemical product (Jobson et al., 2004; Liu et al., 2008), this source was designated as petrochemical industry.

The source contributions to the $O_3$ production rates were obtained from the differences in simulated $O_3$ production rates between a base run and a constrained run. In the base run, the $O_3$ production rate was simulated with the observed concentrations of air pollutants except for the carbonyls, while the concentrations of air pollutants attributable to a specific source were deducted from the observed concentrations for the input of the constrained run. To account for the influence of primary hydrocarbons on the formation of carbonyls, and the subsequent impact on $O_3$ production, carbonyls were not constrained to observations in either the base run or the constrained runs. However, the source-specific primary emissions of carbonyls and their contributions to $O_3$ production were not considered in this approach. Therefore, the source-specific contributions to net $O_3$ production rates were expected to be underestimated, as carbonyls are generally of high $O_3$ formation potentials (Cheng et al., 2010; Dong et al., 2014). The method was applied to each of the six sources, derived from the PMF analysis, thereby acquiring the contribution to $O_3$ production rates of each source.

**Text S3** Definitions of the $O_3$ formation regimes

As shown in Figure 8, $O_3$ formation was divided into VOC$^{\#}$-limited regime and $NO_x$-limited regime with the method used in Lyu et al. (2017). Briefly, at a given $OH\ reactivity_{VOCs^{\#}}$ value, the simulated $O_3$ production rate generally got the maximum at a specific $OH\ reactivity_{NOx}$ value due to the dual role of $NO_x$ in $O_3$ formation. This specific $OH\ reactivity_{NOx}$ value was treated as the dividing point between $NO_x$-limited regime and VOC$^{\#}$-limited regime at the given $OH\ reactivity_{VOCs^{\#}}$ value. Since the scenarios involved 14 gradients of $OH\ reactivity_{VOCs^{\#}}$ (10% - 140% with the step of 10%), 14 pairs of $OH\ reactivity_{NOx}$ and $OH\ reactivity_{VOCs^{\#}}$ were obtained, as shown in the orange crosses in Figure 8. A dividing line was acquired from the linear regression between $OH\ reactivity_{VOCs^{\#}}$ and $OH\ reactivity_{NOx}$ in these scenarios (presented in orange dashed line in Figure 8). $O_3$ formation was limited by VOCs$^{\#}$ and $NO_x$ in the lower right and upper left areas of the dividing line, respectively. Since the horizontal and vertical coordinates were the percentages relative to the average $OH\ reactivity_{VOCs^{\#}}$ and $OH\ reactivity_{NOx}$ during $O_3$ episodes, rather than the actual values of OH reactivity, we did not calculate the dividing ratio of $\frac{OH\ reactivity_{VOCs^{\#}}}{OH\ reactivity_{NOx}}$ here. Further, it was found that the $O_3$ production rates were also enhanced with the increase of

$OH\ reactivity_{VOCs^{\#}}$ in the upper left area close to the dividing line. We defined it as a transitional regime where the $O_3$ formation was comparably sensitive to VOCs# and $NO_x$. Beyond the transitional regime in the upper left area of the dividing line, the sensitivity of $O_3$ formation to $NO_x$ was generally ten times higher than to VOCs#, which was designated as $NO_x$-limited regime. The transitional regime and the $NO_x$-limited regime were divided by the blue dashed line in Figure 8.

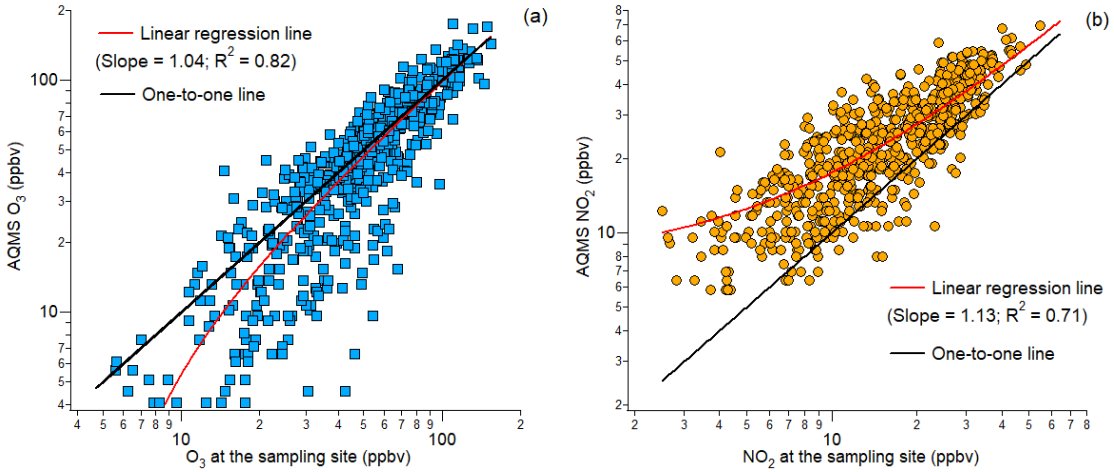


**Figure S1.** Agreement of the hourly (a) $O_3$ and (b) $NO_2$ between our observations on the campus of Shandong University and those monitored at the nearest AQMS by CNEMC.

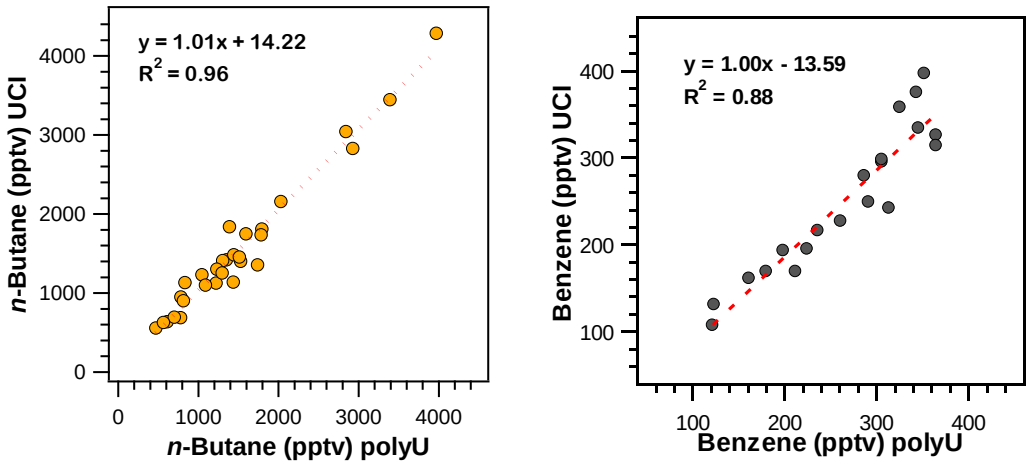

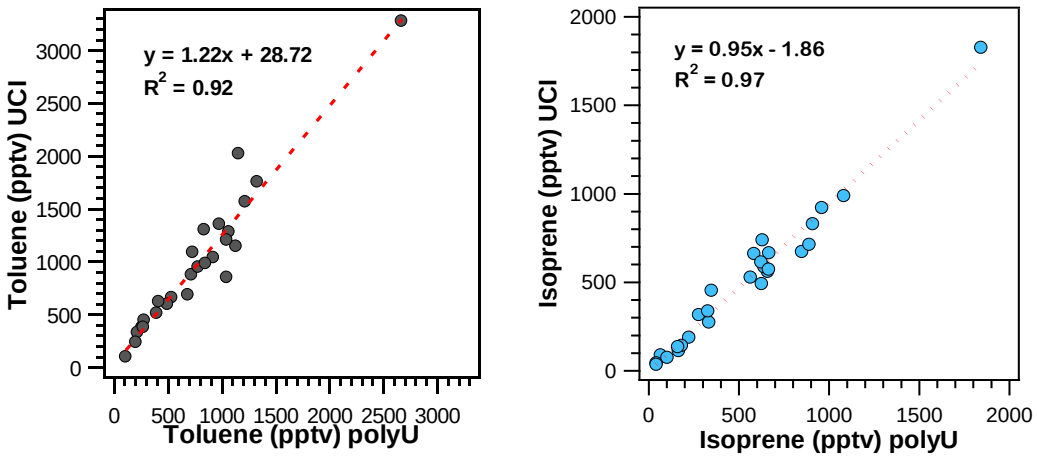


**Figure S2.** Inter-comparison of VOC analysis results between our laboratory (x axis) and Prof. Donald Blake's group (y axis). *n*-butane, benzene, toluene and isoprene are selected as examples. The red dashed line represents the linear regression between VOCs analyzed in two laboratories.

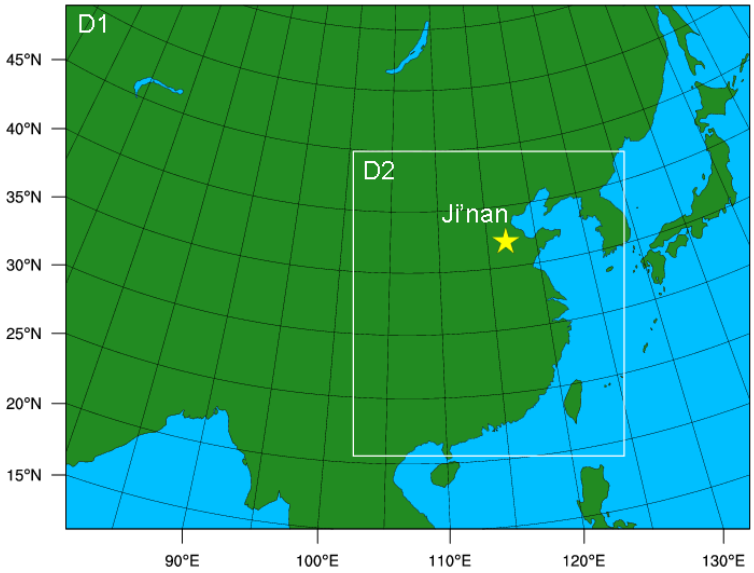


**Figure S3.** Settings of the two-nested domains for the WRF-CMAQ model. D1 and D2 are the outer and inner domains, covering the entire continental area of China and eastern China, respectively. The yellow star represents Ji'nan.

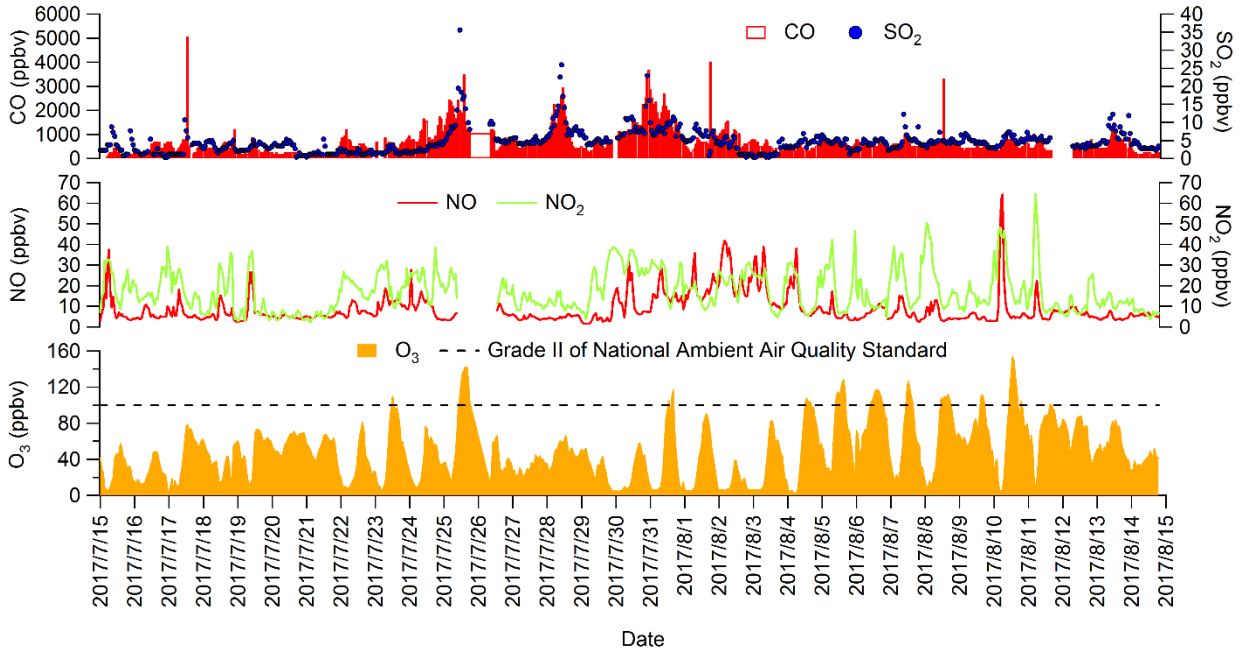


**Figure S4.** Hourly variations of trace gases monitored at the sampling site ($O_3$, NO and $NO_2$) and at the nearest AQMS (CO and $SO_2$) during July 15-August 14, 2017.

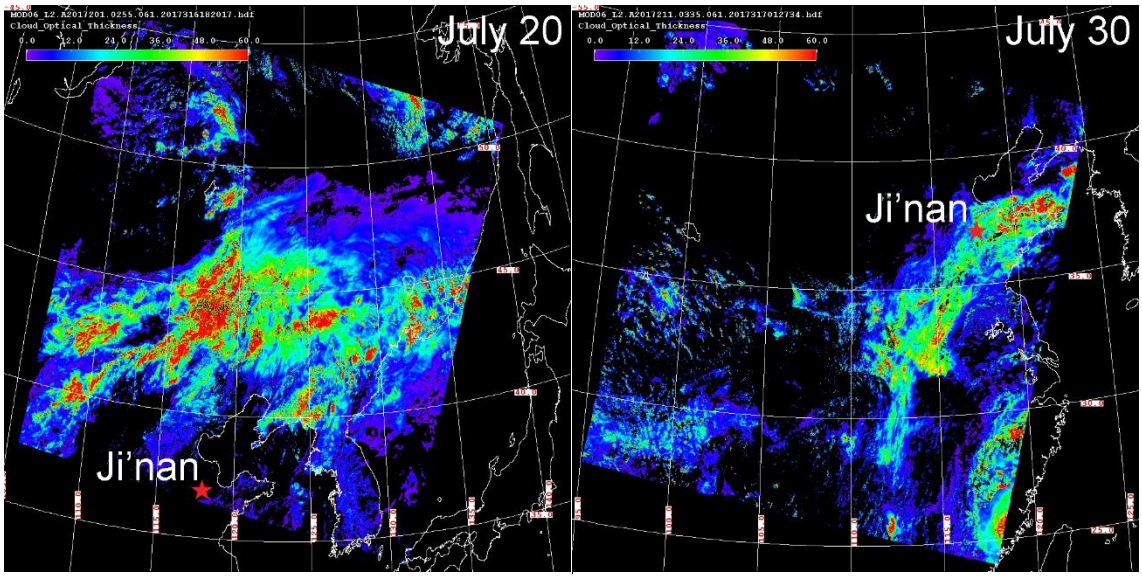

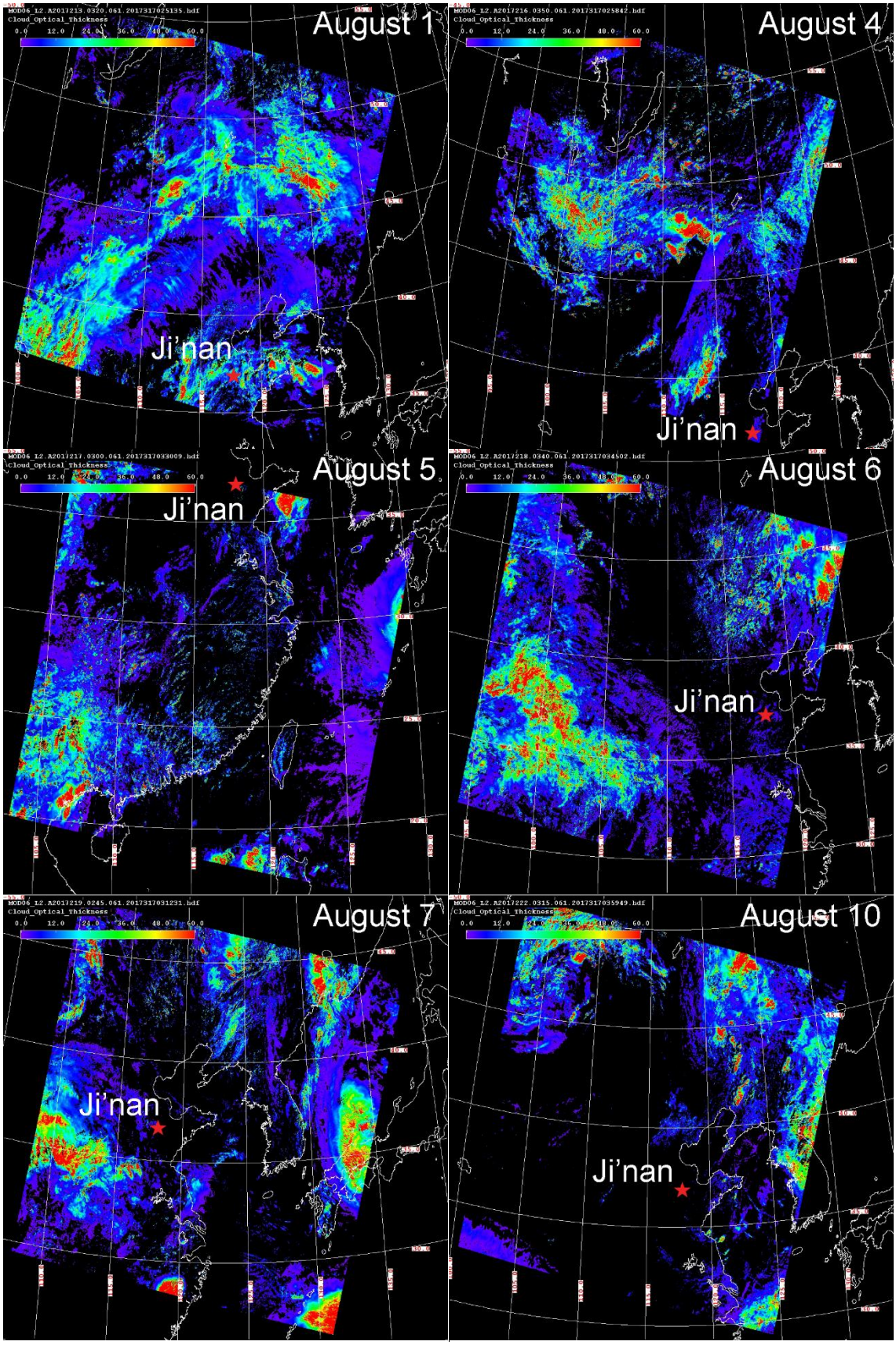
August 1
Ji'nan
August 4
Ji'nan
August 5
Ji'nan
August 6
Ji'nan
August 7
Ji'nan
August 10
Ji'nan

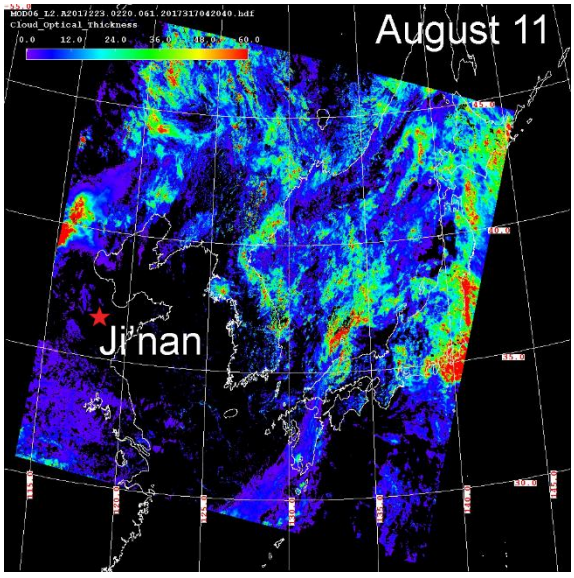


**Figure S5.** Cloud optical depth (COD) retrieved from terra/MODIS at noon (10:30 – 12:00 LT) of the canister sampling days. The color scale denotes for the COD within the range of 0 (purple) to 60 (red). The red star denotes Ji'nan.

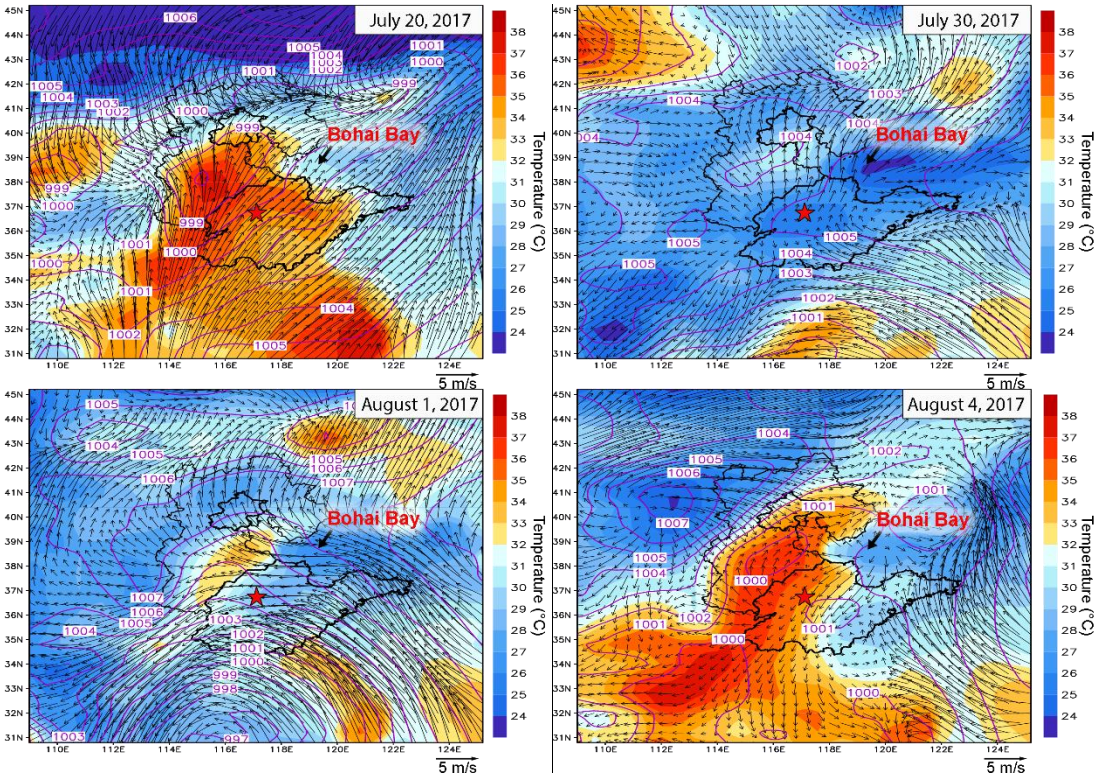

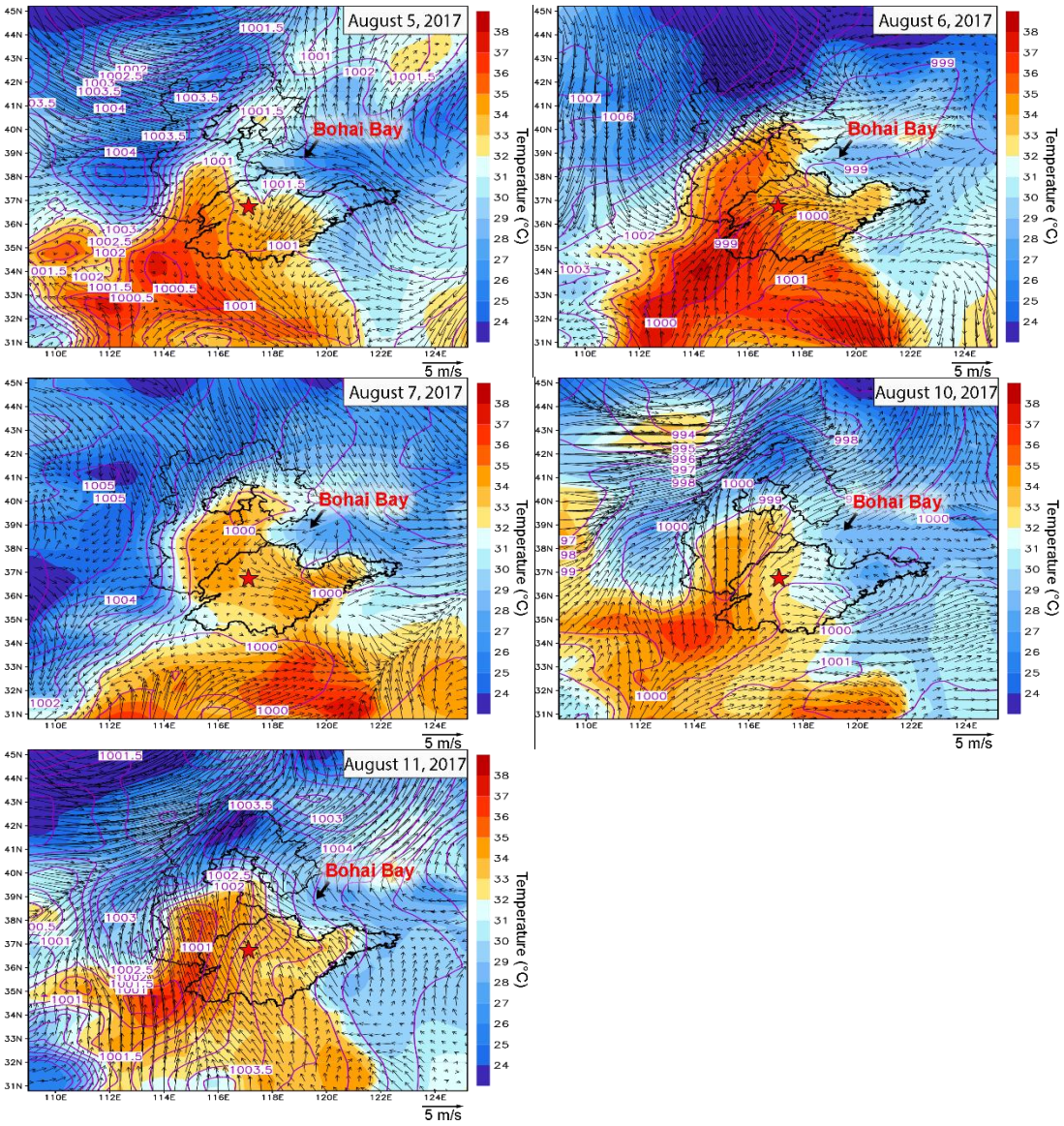


**Figure S6.** Weather charts at 14:00 LT on individual VOC sampling days. The red star denotes for Ji'nan. The dark black line is the boundary of Shandong province. Bohai Bay is located to the northeast of Shandong province. Numbers in the figure are sea-level pressures in unit of hPa.

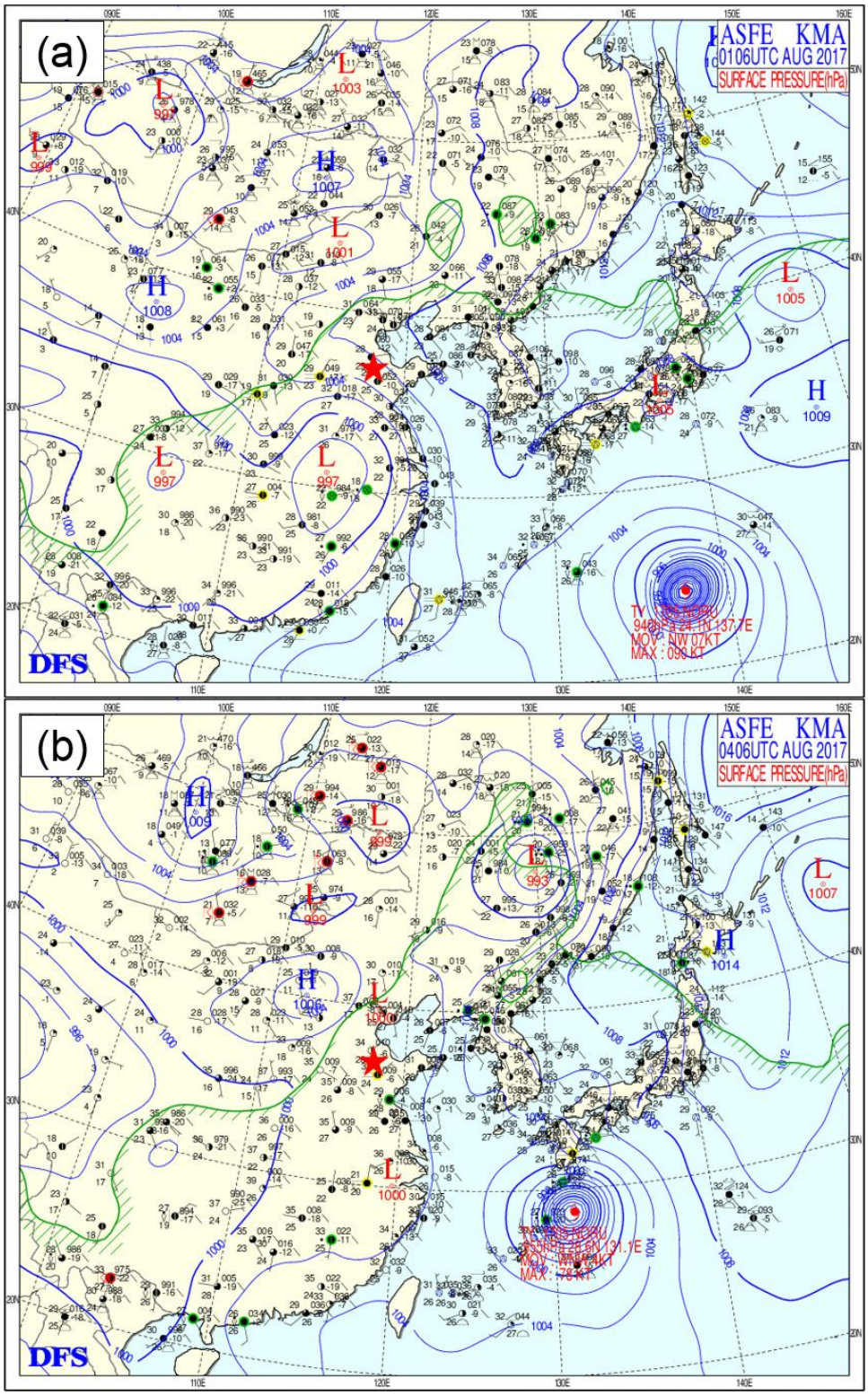
(a)
ASFE KMA
0106UTC AUG 2017
SURFACE PRESSURE(hPa)
DFS
(b)
ASFE KMA
0406UTC AUG 2017
SURFACE PRESSURE(hPa)
DFS

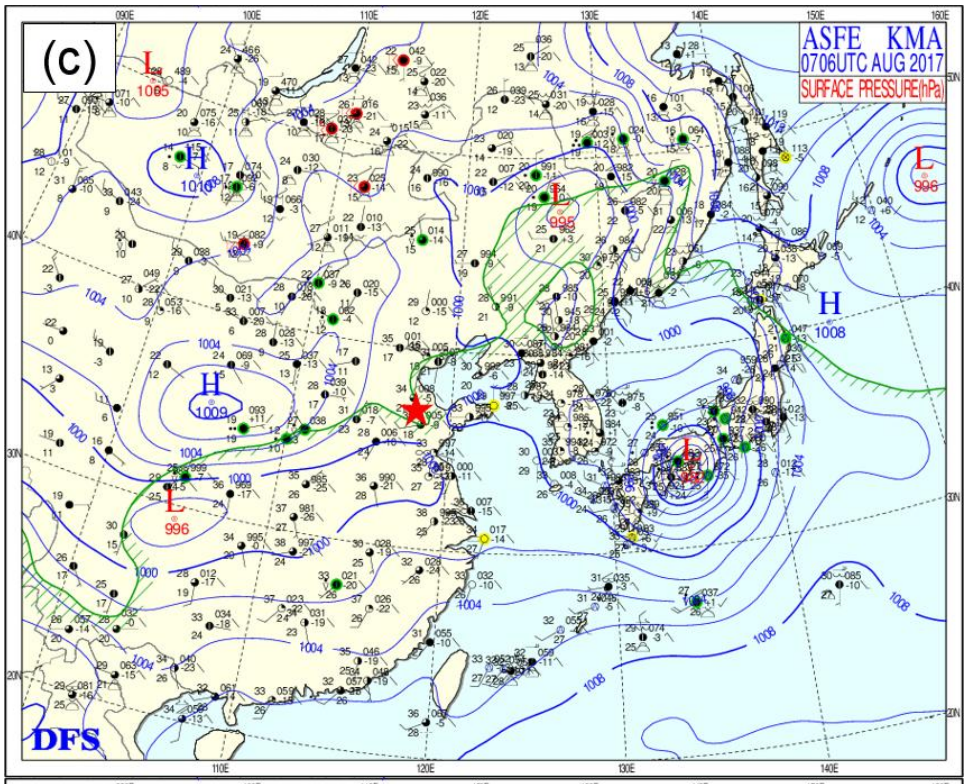
(c)
ASFE KMA
0706UTC AUG 2017
SURFACE PRESSURE(hPa)
DFS

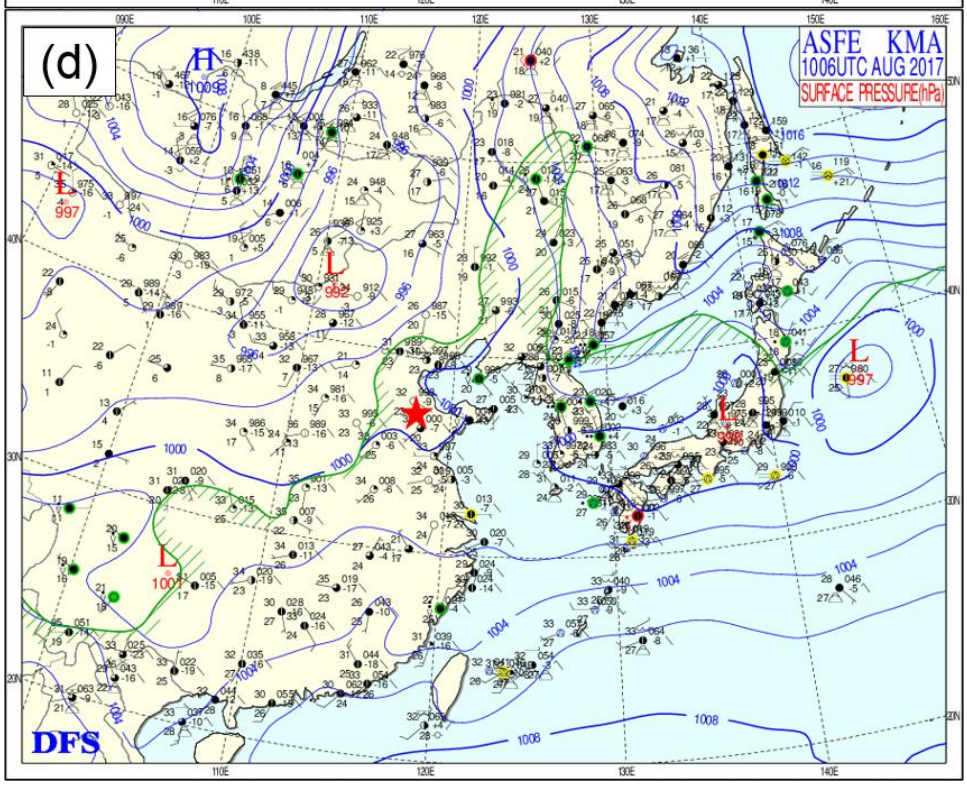
(d)
ASFE KMA
1006UTC AUG 2017
SURFACE PRESSURE(hPa)
DFS

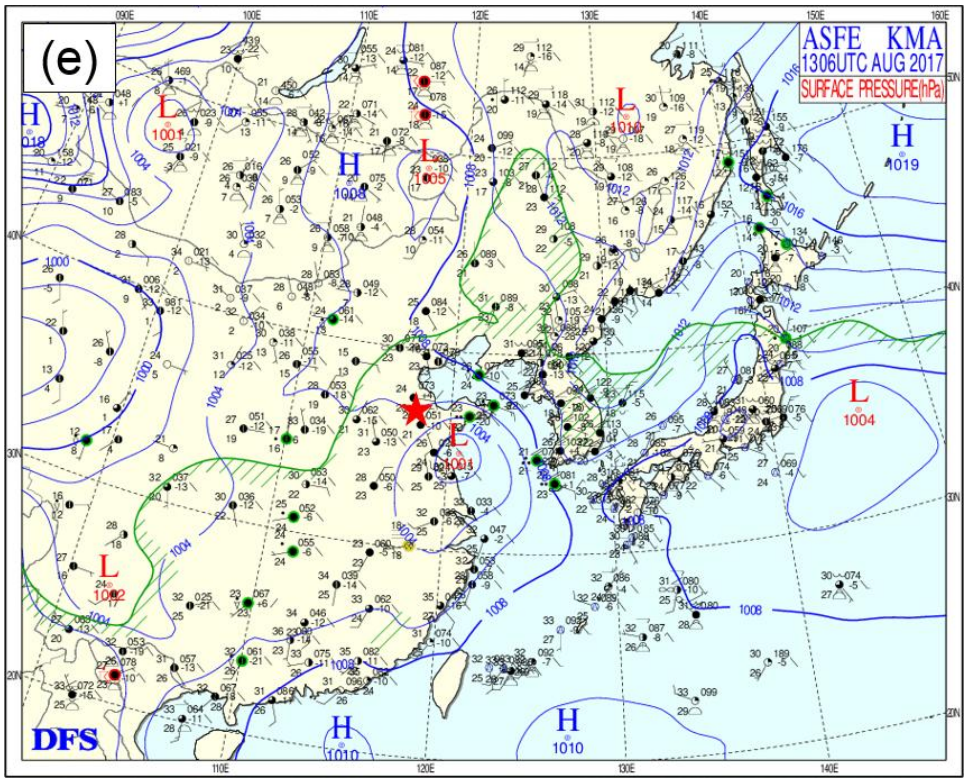


**Figure S7.** Weather chart over the Northeast Asia on (a) August 01, (b) August 04, (c) August 07, (d) August 10 and (e) August 13 at 06:00 UTC (14:00 LT) at surface level. The red star denotes Ji'nan city. The capital letters "H" and "L" represent high pressure center and low pressure center, respectively. Blue lines are the sea level isobars. Green line is the isometric humidity line with the specific humidity of ≥15g/kg on the grid side. All the charts can be accessed through the link: http://222.195.136.24/forecast.html.

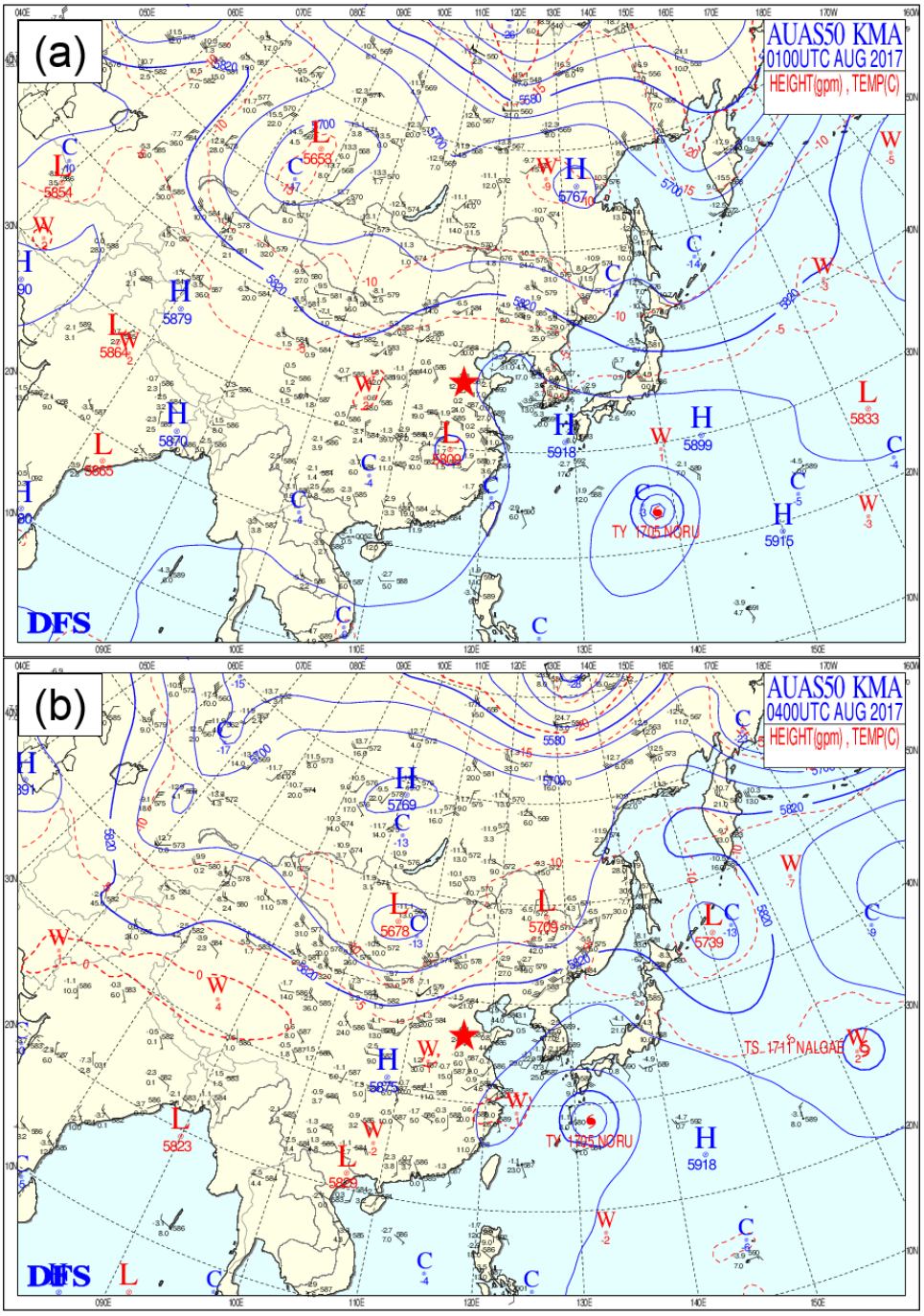
(a)
AUAS50 KMA
0100UTC AUG 2017
HEIGHT(gpm) , TEMP(C)
TY 1705 NORU
DFS
(b)
AUAS50 KMA
0400UTC AUG 2017
HEIGHT(gpm) , TEMP(C)
TS 1711 NALGAE
TY 1705 NORU
DFS

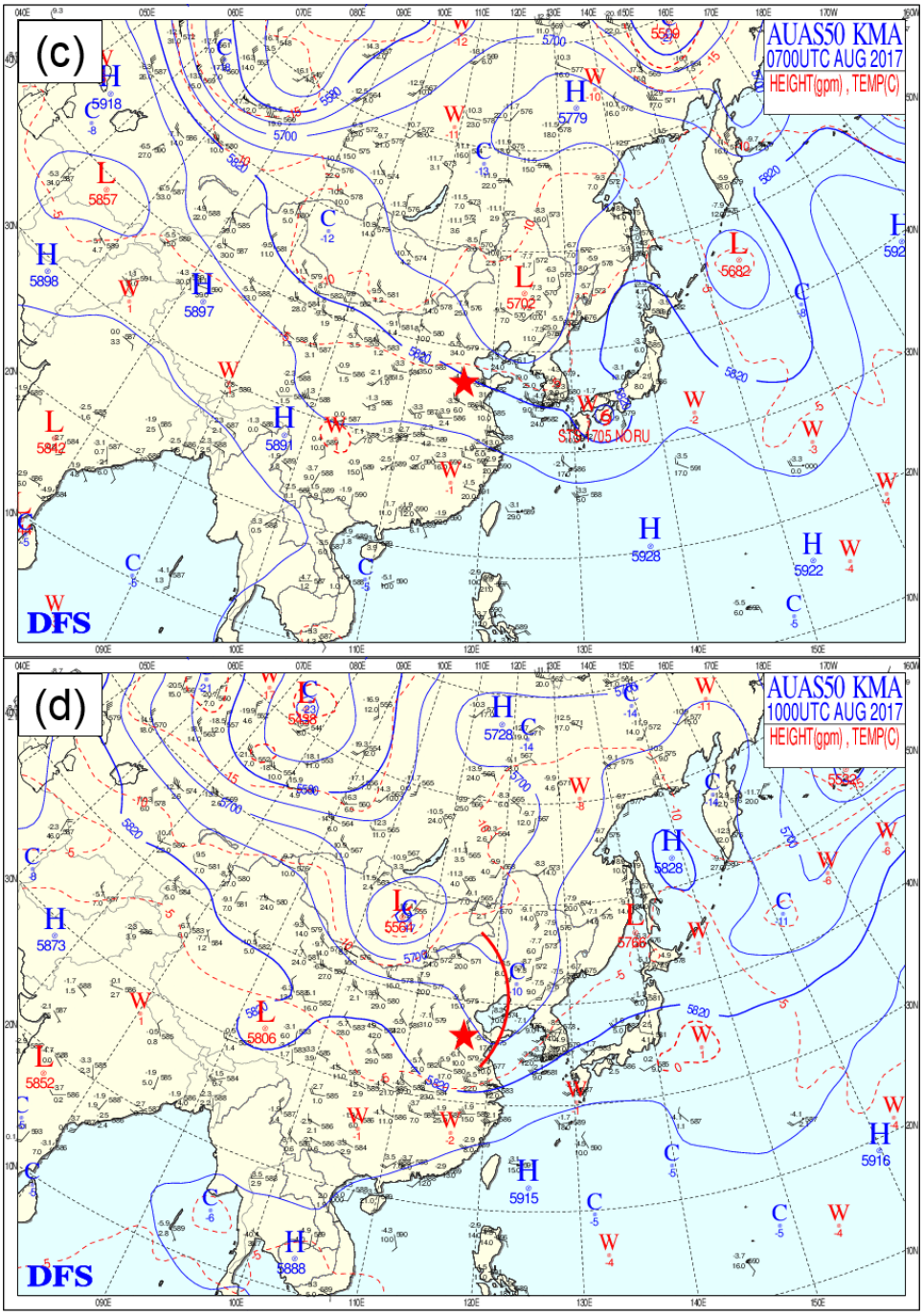
(c)
AUAS50 KMA
0700UTC AUG 2017
HEIGHT(gpm) , TEMP(C)
DFS
(d)
AUAS50 KMA
1000UTC AUG 2017
HEIGHT(gpm) , TEMP(C)
DFS

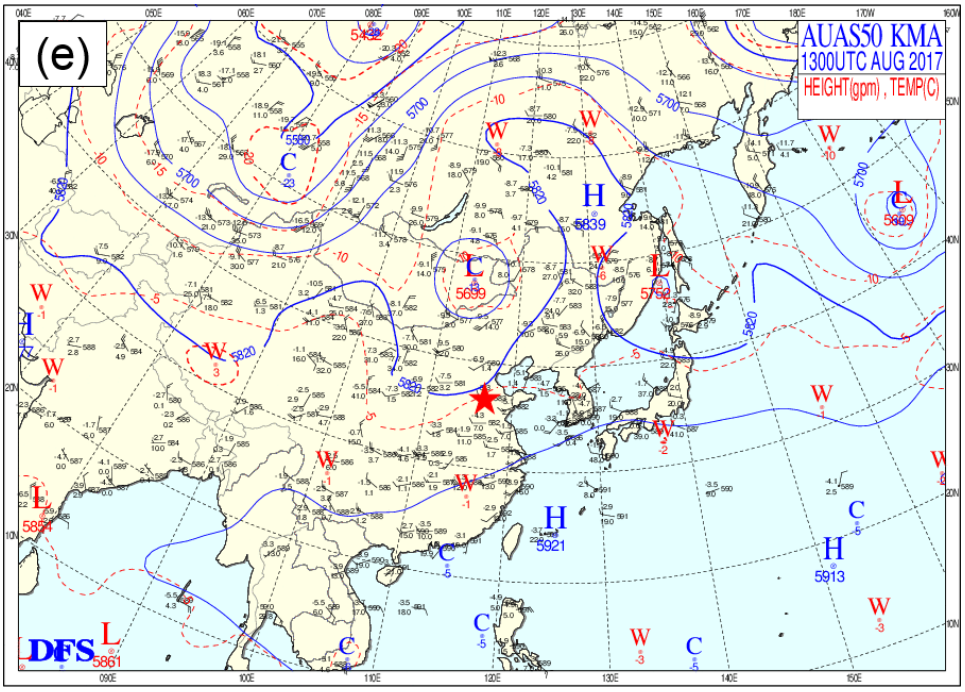


**Figure S8.** Weather chart over the Northeast Asia on (a) August 01, (b) August 04, (c) August 07, (d) August 10 and (e) August 13 at 00:00 UTC (08:00 LT) at altitude of 500 hPa. The red star denotes Ji'nan city. The capital letters "H" and "L" represent high pressure center and low pressure center, respectively. Blue lines are the 500 hPa geopotential height (gpm) lines. The red curve in panel (d) demonstrates the low pressure trough. All the charts can be accessed through the link: http://222.195.136.24/forecast.html.

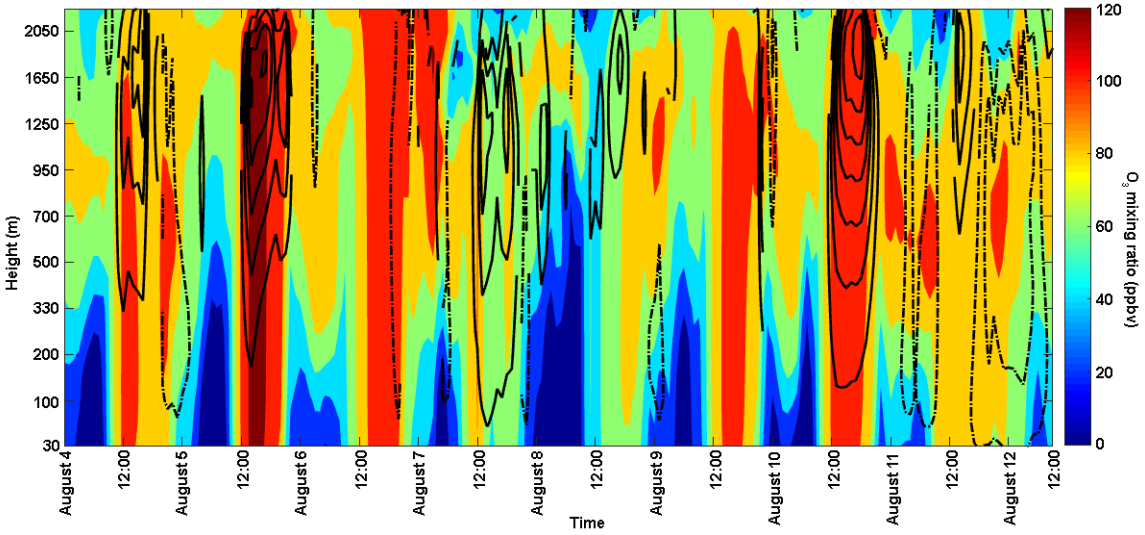


**Figure S9.** Vertical profile of the simulated $O_3$ over Ji'nan during August 4-11. The black solid and dotted lines represent the updraft and downdraft simulated by WRF-CMAQ, respectively. The areas with no line indicate that there were no simulated winds in vertical direction.

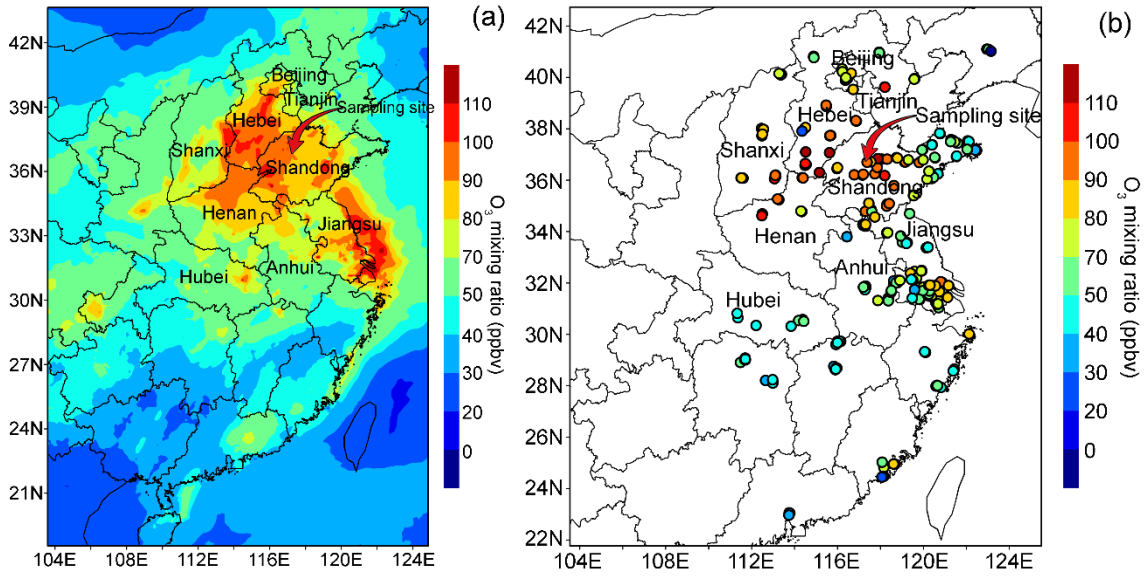


**Figure S10.** Comparison between the spatial distributions of (a) the WRF-CMAQ simulated $O_3$ and (b) the observed $O_3$ at 14:00 LT averaged over August 4-11. The observed $O_3$ is acquired from the AQMSs of CNEMC.

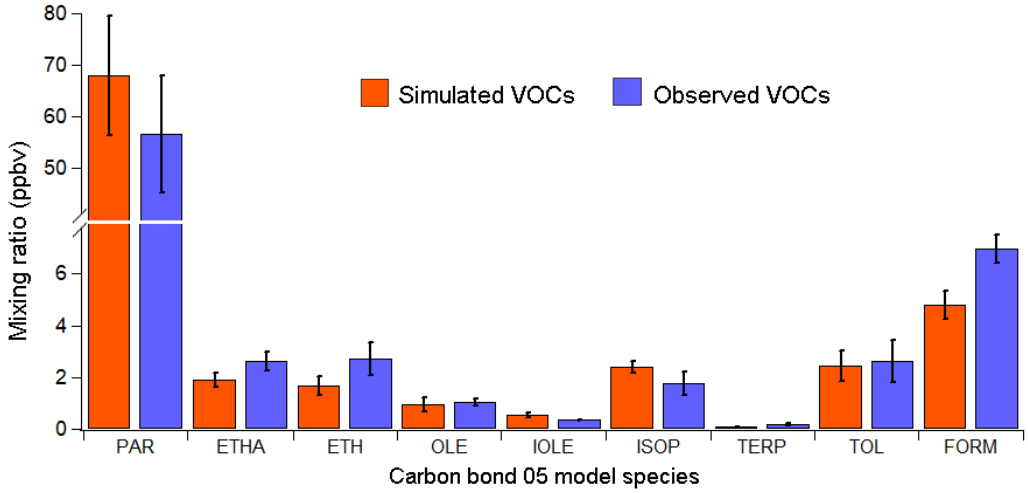


**Figure S11.** Comparison between the averages of the hourly observed and WRF-CMAQ simulated VOCs. PAR: paraffin carbon bond; ETHA: ethane; ETH: ethene; OLE: terminal olefin carbon bond; IOLE: internal olefin carbon bond; ISOP: isoprene; TERP: terpene; TOL: toluene and other monoalkyl aromatics; FORM: formaldehyde. The matrix of assignments from real compounds to carbon bond 05 model species can be found in Yarwood et al. (2005).

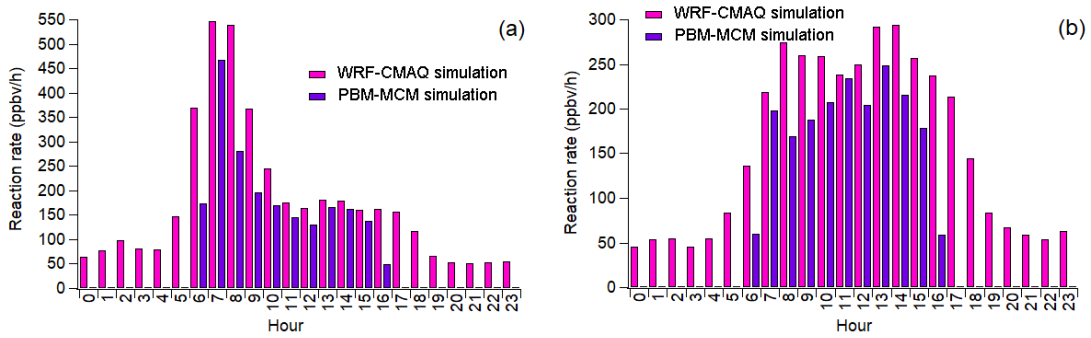


**Figure S12.** Average diurnal cycle of "NO+$O_3$" reaction rates simulated by WRF-CMAQ and PBM-MCM during (a) $O_3$ episodes and (b) non-episodes.

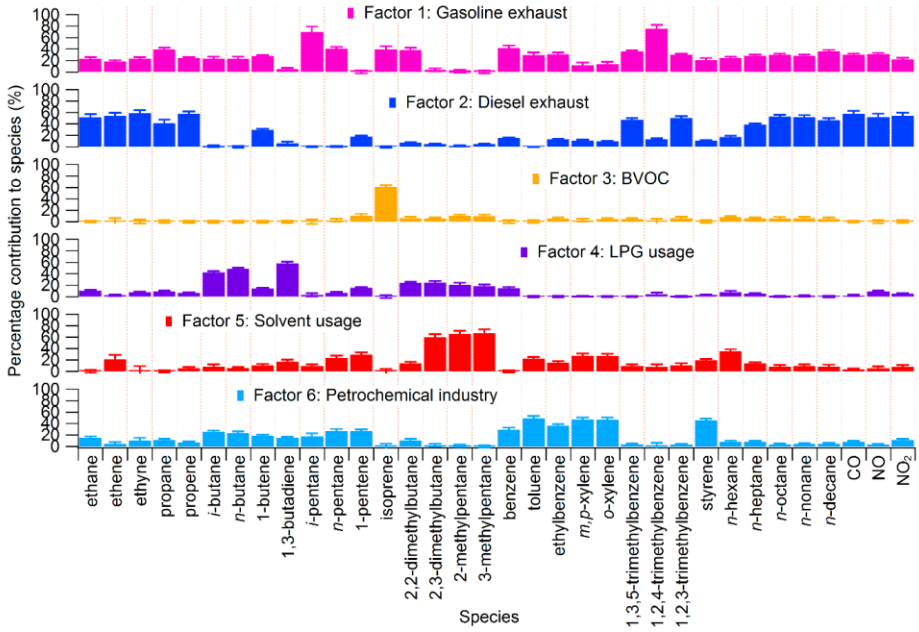


**Figure S13.** Profiles of the six sources of $O_3$ precursors identified for the samples collected in daytime of the VOC sampling days in Ji'nan.

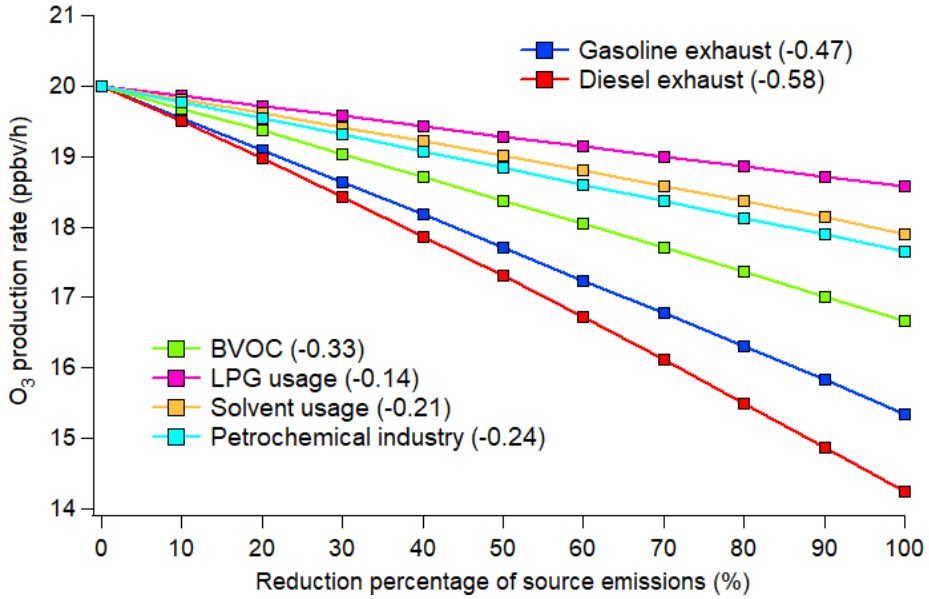


**Figure S14.** Average $O_3$ production rate at 12:00 LT during $O_3$ episodes as a response of the reduction percentages of source emissions. Numbers in the brackets are the average $O_3$ reduction efficiencies (ppbv/10% reduction in source emissions).

| Species | Site | Instrument | Resolution | Accuracy | Precision | Detection limit |
|---|---|---|---|---|---|---|
| $SO_2$ | AQMS* | API, Model 100 E | 20 sec | <20% | 0.5% of reading above 50 ppbv | 0.4 ppbv |
| CO | AQMS | API, Model 300 E | 10 sec | <20% | 0.5% of reading | 40 ppbv |
| NO-$NO_2$-$NO_x$ | AQMS | API, model 200E | 20 sec | <20% | 0.5% of reading | 0.4 ppbv |
| | Campus site # | Thermo, Model 42C | 1 min | <15% | 0.4 ppbv | 0.4 ppbv |
| $O_3$ | AQMS | API, model 400E | 10 sec | <20% | <0.5% of reading | 0.6 ppbv |
| | Campus site | Thermo, Model 49C | 20 sec | <15% | 1.0 ppbv | 1.0 ppbv |

* An air quality monitoring station of China National Environmental Monitoring Center closest to our sampling site in the campus of Shandong University; # Our sampling site on the campus of Shandong University.

**Table S1.** Descriptions of the trace gas analyzers used in this study.

| Date | Episode/Non-episode | $J(O^1D)$ ($s^{-1}$) | $JNO_2$ ($s^{-1}$) |
|---|---|---|---|
| July 20 | Non-episode | $3.40 \times 10^{-5}$ | $9.27 \times 10^{-3}$ |
| July 30 | Non-episode | $1.02 \times 10^{-5}$ | $2.73 \times 10^{-3}$ |

| | | | |
|---|---|---|---|
| August 1 | Non-episode | $2.71 \times 10^{-5}$ | $7.50 \times 10^{-3}$ |
| August 4 | Episode | $2.85 \times 10^{-5}$ | $7.95 \times 10^{-3}$ |
| August 5 | Episode | $2.69 \times 10^{-5}$ | $7.50 \times 10^{-3}$ |
| August 6 | Episode | $2.75 \times 10^{-5}$ | $7.70 \times 10^{-3}$ |
| August 7 | Episode | $2.34 \times 10^{-5}$ | $6.52 \times 10^{-3}$ |
| August 10 | Episode | $3.07 \times 10^{-5}$ | $8.72 \times 10^{-3}$ |
| August 11 | Episode | $2.90 \times 10^{-5}$ | $8.25 \times 10^{-3}$ |

**Table S2.** Daily maximum photolysis rates of $O_3$ and $NO_2$ on VOC sampling days in Ji'nan.

| OH reactivity of species X | Full name of species/VOC groups | Species included |
|---|---|---|
| RNO | Nitric oxide | Nitric oxide |
| RNO2 | Nitrogen dioxide | Nitrogen dioxide |
| RCO | Carbon monoxide | Carbon monoxide |
| RCarbonyls | Carbonyls | Formaldehyde, acetaldehyde, acetone, hexanal |
| RBVOCs | Biogenic VOCs | Isoprene, *α*-pinene, *β*-pinene |
| RAromatics | Aromatics | Benzene, toluene, ethylbenzene, *m*/*p*-xylenes, *o*-xylene |
| RAlkenes | Alkenes | Ethene, ethyne, propene, 1-/*i*-butene, 1,3-butadiene, *trans*-2-butene, *cis*-2-butene, 1-pentene |
| RAlkanes | Alkanes | Ethane, propane, *n*/*i*-butanes, *n*/*i*-pentanes |

**Table S3.** Full name of inorganic trace gases and VOC species for the calculation of OH reactivity.

| Meteorological parameter/Air pollutant | Avg. Obs. | Avg. Sim. | Diff. | RMSE | NMB | NME | IOA |
|---|---|---|---|---|---|---|---|
| Temp. (°C) | 30.0 | 30.7 | 0.7 | 2.4 | 0.02 | 0.06 | 0.89 |
| R.H. (%) | 72.7 | 67.5 | -5.2 | 14.4 | -0.06 | 0.15 | 0.82 |
| W.S. (m/s) | 2.8 | 3.3 | 0.5 | 1.5 | 0.38 | 0.56 | 0.74 |
| Press. (hPa) | 1000.5 | 998.8 | -1.7 | 4.0 | -0.002 | 0.003 | 0.56 |
| $NO_2$ (ppbv) | 26.7 | 28.4 | 1.7 | 16.7 | 0.18 | 0.58 | 0.73 |
| $O_3$ (ppbv) | 62.8 | 52.4 | -10.4 | 24.0 | -0.07 | 0.48 | 0.89 |

**Table S4.** Statistical comparisons of the WRF-CMAQ simulated and observed meteorological parameters, $O_3$ and $NO_2$. The comparisons are made for the hourly data in 24 hours on all the VOC sampling days.

| $O_3$ production pathway | $O_3$ destruction pathway |
|---|---|
| $HO_2 + NO$ | $OH + NO_2$ |
| $RO_2 + NO$ | $O^1(D) + H_2O$ |
| | $O_3 + OH$ |
| | $O_3 + HO_2$ |
| | $O_3$ + alkenes |

**Table S5.** Production and destruction pathways of $O_3$.

**References:**


Dong, D., Shao, M., Li, Y., Lu, S., Wang, Y., Ji, Z., and Tang, D.: Carbonyl emissions from heavy-duty diesel vehicle exhaust in China and the contribution to ozone formation potential, J. Environ. Sci., 26(1), 122-128, **2014**.

Guenther, A., Karl, T., Harley, P., Wiedinmyer, C., Palmer, P.I., and Geron, C.: Estimates of global terrestrial isoprene emissions using MEGAN (Model of Emissions of Gases and Aerosols from Nature), Atmos. Chem. Phys., 6(11), 3181-3210, **2006**.

Guo, H., Cheng, H.R., Ling, Z.H., Louie, P.K., and Ayoko, G.A.: Which emission sources are responsible for the volatile organic compounds in the atmosphere of Pearl River Delta?, J. Hazard. Mat., 188(1-3), 116-124, **2011**.

Ho, K.F., Lee, S.C., Ho, W.K., Blake, D.R., Cheng, Y., Li, Y.S., Ho, S.S., Fung, K., Louie, P.K., and Park, D.: Vehicular emission of volatile organic compounds (VOCs) from a tunnel study in Hong Kong, Atmos. Chem. Phys., 9(19), 7491-7504, **2009**.

Hu, J., Chen, J., Ying, Q., and Zhang, H.: One-year simulation of ozone and particulate matter in China using WRF/CMAQ modeling system, Atmos. Chem. Phys., 16(16), 10333–10350, **2016**.

Jiang, F., Guo, H., Wang, T.J., Cheng, H.R., Wang, X.M., Simpson, I.J., Ding, A.J., Saunders, S.M., Lam, S.H.M., and Blake, D.R.: An ozone episode in the Pearl River Delta: Field observation and model simulation, J. Geophys. Res. – Atmos., 115(D22), **2010**.

Jobson, B.T., Berkowitz, C.M., Kuster, W.C., Goldan, P.D., Williams, E.J., Fesenfeld, F.C., Apel, E.C., Karl, T., Lonneman, W.A., and Riemer, D.: Hydrocarbon source signatures in Houston, Texas: Influence of the petrochemical industry, J. Geophys. Res. – Atmos., 109(D24), doi.org/10.1029/2004JD004887, **2004**.

Ling, Z.H. and Guo, H.: Contribution of VOC sources to photochemical ozone formation and its control policy implication in Hong Kong, Environ. Sci. Policy, 38, 180-191, **2014**.

Liu, Y., Shao, M., Fu, L., Lu, S., Zeng, L., and Tang, D.: Source profiles of volatile organic compounds (VOCs) measured in China: Part I, Atmos. Environ., 42(25), 6247-6260, **2008**.

Lyu, X.P., Guo, H., Wang, N., Simpson, I.J., Cheng, H.R., Zeng, L.W., Saunders, S.M., Lam, S. H.M., Meinardi, S., and Blake, D.R.: Modeling C1-C4 alkyl nitrate photochemistry and their impacts on O3 production in urban and suburban environments of Hong Kong, J. Geophys. Res. – Atmos., 122(19), **2017**.

Paatero, P. and Tapper, U.: Positive matrix factorization: A non-negative factor model with optimal utilization of error estimates of data values, Environmetrics, 5(2), 111-126, **1994**.

Song, Y., Dai, W., Shao, M., Liu, Y., Lu, S., Kuster, W., and Goldan, P.: Comparison of receptor models for source apportionment of volatile organic compounds in Beijing, China, Environ. Pollut., 156(1), 174-183, **2008**.

Wang, N., Guo, H., Jiang, F., Ling, Z.H., and Wang, T.: Simulation of ozone formation at different elevations in mountainous area of Hong Kong using WRF-CMAQ model, Sci. Total Environ., 505, 939-951, **2015**.

Willmott, C.J., Ackleson, S.G., Davis, R.E., Feddema, J.J., Klink, K.M., Legates, D.R., O'Donnell, J., and Rowe, C.M.: Statistics for the evaluation and comparison of models, J. Geophys. Res. - Oceans, 90(C5), 8995-9005, **1985**.